DOI: 10.1002/chem.201001473

Chemical Bonding in Compounds of the $CuAl_2$ Family: $MnSn_2$, $FeSn_2$ and $CoSn_2$

Marc Armbrüster,* Walter Schnelle, Raul Cardoso-Gil, and Yuri Grin[a]

Abstract: A model for the chemical bonding in the isostructural intermetallic compounds $MnSn_2$, $FeSn_2$ and $CoSn_2$, crystallising in the $CuAl_2$-type structure, is developed. The description is based on quantum-chemical calculations applying the electron localisability approach as well as on experimental results obtained from Raman spectroscopy, Hall effect and electrical resistivity measurements on oriented single crystals. The analysis of the chemical bonding reveals four different covalent interactions leading to the formation of interpenetrating 6^3 nets of tin and chains of transition-metal atoms T (T = Mn, Fe or Co) along [001], which are interconnected by three-centre bonds. Polarised Raman measurements on oriented single crystals allowed the determination of the bond strengths, resulting in a bond order of 0.5 within the 6^3 nets, while the three-centre interactions show bond orders of up to 1. Measurements show a metal-like temperature dependence of the resistivity. A comparison of the results with the bonding models obtained for the isostructural compounds $CuAl_2$, $TiSb_2$ and VSb_2 reveals the influence of the main-group element on the connectivity pattern.

Keywords: quantum chemistry · Raman spectroscopy · solid-state structures · tin · transition metals

Introduction

Because of their special physical properties, the stannides $MnSn_2$,[1,2] $FeSn_2$[2–4] and $CoSn_2$[5] have several potential uses. The suggested applications range from data storage[6] and sensors[6] to electrodes in rechargeable batteries.[7–11]. In addition, $FeSn_2$ plays a role as mediating layer in the tinning process.[12,13]

Understanding the origin of the properties on an atomic level is necessary to optimise these materials in a rational way. Since the chemical and physical properties depend strongly on the chemical bonding, it is crucial to investigate the atomic interactions. A recent example is the understanding of the in situ stability of Pd–Ga intermetallic compounds, which are highly selective hydrogenation catalysts.[14,15]

The intermetallic compounds $MnSn_2$, $FeSn_2$ and $CoSn_2$ cannot be classified within the known bonding concepts after Zintl–Klemm,[16–21] Hume-Rothery[22–26] or Laves,[27–29] so the prediction of atomic interactions in these compounds is not straightforward. All three TSn_2 (T = Mn, Fe, Co) compounds crystallise in the $CuAl_2$ type of crystal structure (space group *I*4/*mcm*, T in 4*a*, Sn in 8*h*) and the crystal structures have been recently reinvestigated.[30–32] By focusing on the homoatomic Sn–Sn interactions, the structure can be described in at least three different ways: 1) as a three-dimensional network of connected tetrahedral stars,[33–35] 2) as layered $3^2.4.3.4$ nets[35,36] or 3) as interpenetrating graphite-like 6^3 nets.[35,37] In these descriptions, which are based on purely geometrical considerations of the interatomic distances, the T atoms are placed in channels extending along the [001] direction. An alternative way to describe the structure evolves when only the heteroatomic interactions T–Sn are taken into account. The structure then consists of T atoms surrounded by 8 Sn atoms, which form a quadratic antiprism. These antiprisms are stacked along the fourfold axis and possess common edges, thus building a three-dimensional network.[35]

Investigations of the chemical bonding in $CuAl_2$ applying an electron-localisability function revealed 6^3 nets built up by Al and three-centre Cu-Al-Cu bonding.[30,38] The isostructural antimonides $TiSb_2$ and VSb_2 on the other hand, possess Sb_2 dumbbells instead of 6^3 nets, while keeping the three-centre interactions. In addition, Ti–Ti and V–V interactions were present, thus forming transition-metal chains along [001].[30,39] Up to now, the description of the chemical bonding in the stannides was based on the interatomic distances, leading to the postulation of 6^3 nets formed by tin atoms as

[a] Dr. M. Armbrüster, Dr. W. Schnelle, Dr. R. Cardoso-Gil, Prof. Y. Grin
Max-Planck-Institut für Chemische Physik fester Stoffe
Nöthnitzer Str. 40, 01187 Dresden (Germany)
Fax: (+49) 351-46464002
E-mail: research@armbruester.net

well as T chains along [001].[37] In contrast to these considerations, several Mössbauer investigations indicate also heteroatomic T–Sn interactions.[40–46]

Here we present the results of an experimental as well as quantum chemical study of the chemical bonding in the isostructural compounds $MnSn_2$, $FeSn_2$ and $CoSn_2$. The synthesis of single-phase polycrystalline materials and single crystals of the compounds is reported. The phase boundaries were established and polarised Raman spectroscopy as well as directional measurements of the Hall effect and the electrical resistivity were performed on single crystals. To understand the observations, the atomic interactions were investigated applying the electron localisability approach and as a result, a consistent bonding model, including the strength of the bonds in the compounds, was developed.

Results and Discussion

Phase stability and homogeneity ranges: Since the physical properties of intermetallic compounds may depend strongly on their composition and more or less pronounced homogeneity ranges are frequently observed for this class of inorganic materials, we start our investigation with the determination of the phase boundaries of the compounds. Three kinds of samples were synthesised: samples 1 with nominal composition $T_{20}Sn_{80}$ (T = Mn, Fe or Co), samples 2 with nominal composition $T_{40}Sn_{60}$ and single-phase samples 3 with the composition $T_{33}Sn_{67}$. The width of the homogeneity range was determined from the two-phase samples 1 and 2 synthesised at 500 °C, while the formation temperatures were measured on sample 3.

During the investigation of the homogeneity ranges, it was observed that the compound $MnSn_2$ is not stable in air, but corrodes slowly to elemental Sn—mostly in the form of whiskers[47,48]—and manganese hydroxides and oxides. This observation explains earlier reports, claiming that $MnSn_2$ cannot be synthesised without containing elemental Sn.[49–51] For the investigations reported here, the $MnSn_2$-containing samples were prepared, handled and stored in inert argon atmosphere to avoid oxidation and hydrolysis.

The results from the WDXS measurements as well as the determined lattice parameters for the TSn_2 compounds are shown in Table 1.

Table 1. Compositions and lattice parameters of the TSn_2 phases.

Nominal composition	WDXS	a [Å]	c [Å]
$Mn_{20}Sn_{80}$	$Mn_{32.2(5)}Sn_{67.8(5)}$	6.6613(3)	5.4396(7)
$Mn_{33}Sn_{67}$	$Mn_{0.97(1)}Sn_2$	6.6616(1)	5.4396(6)
$Mn_{40}Sn_{60}$	$Mn_{32.7(2)}Sn_{67.3(2)}$	6.6613(3)	5.4415(8)
$Fe_{20}Sn_{80}$	$Fe_{32.74(6)}Sn_{67.26(6)}$	6.530(2)	5.325(3)
$Fe_{33}Sn_{67}$	$Fe_{0.99(1)}Sn_2$	6.533(1)	5.320(2)
$Fe_{40}Sn_{60}$	$Fe_{33.18(9)}Sn_{66.82(9)}$	6.533(1)	5.320(2)
$Co_{20}Sn_{80}$	$Co_{32.94(2)}Sn_{67.16(2)}$	6.362(1)	5.457(2)
$Co_{33}Sn_{67}$	$Co_{0.99(1)}Sn_2$	6.361(4)	5.4581(6)
$Co_{40}Sn_{60}$	$Co_{33.09(7)}Sn_{66.91(5)}$	6.3625(3)	5.4563(3)

According to these results, the three compounds possess small homogeneity ranges (< 0.5 at. %) and, thus, can be regarded as line compounds. This is corroborated by our results on $CuAl_2$, for which the homogeneity range is clearly seen from the difference in the lattice parameters on the Cu-rich and Cu-poor side. The determined, nearly ideal compositions of $Mn_{0.97(1)}Sn_2$, $Fe_{0.99(1)}Sn_2$ and $Co_{0.99(1)}Sn_2$ are in accordance with earlier reports.[3,52–54]

DSC measurements on the single-phase samples revealed decomposition temperatures of 555(2)°C and 531(2)°C for $MnSn_2$ and $FeSn_2$, respectively. Although the former is in good agreement with the reported value for $MnSn_2$ (549(2)°C[52]), the value determined for $FeSn_2$ is 35 °C higher than reported earlier.[3] $CoSn_2$ is formed at 556(2)°C, which lies within the range of earlier reported temperatures (500–571 °C[2,55–58]).

Since for $FeSn_2$ there is a large discrepancy between the reported (7.446–7.743 $g\,cm^{-3}$[3,4,12]) and crystallographic density (8.578 $g\,cm^{-3}$[31]), the density of $FeSn_2$ was re-determined. The obtained value of 8.56(1) $g\,cm^{-3}$ is in very good agreement with the value calculated for the ideal composition $FeSn_2$.

To exclude the existence of low-temperature modifications, single crystals of the compounds were enclosed in evacuated quartz glass ampoules and treated at 150 °C for 14 months. A comparison of the crystallographic data, obtained from single crystal X-ray structure analysis (Table 2), show no significant deviation from the structural information published earlier.[30–32]

Physical properties: All three compounds possess bright metal lustre and are very brittle, characteristic for many intermetallic compounds. As reported before, Raman spectroscopy on intermetallic phases is possible despite their metal-like appearance.[30,38,39] Raman spectroscopy was performed on powders, obtained by grinding single crystals, as well as on oriented single crystals. A factor group analysis of the crystal structure reveals five Raman active modes ($A_{1g} + B_{1g} + B_{2g} + 2E_g$, for details see references [30,38]). All of them were observed and the symmetry of the modes was identified by polarised Raman measurements on oriented single crystals (Figure 1).

To gather information on the charge carrier concentration and the electrical conductivity of the compounds, Hall effect measurements were carried out. To determine the components of the Hall effect and resistivity tensors, single-crystalline slabs were prepared. Since the crystals of $FeSn_2$ possessed a needle-like morphology, only the R_{132} and ρ_{33} component of the Hall effect and resistivity tensors, respectively, could be determined (notation according to reference [59]). The results of the measurements are given in Figure 2.

All three compounds show a metal-like temperature dependence of the electrical resistivity. While for $MnSn_2$ and $FeSn_2$ the resistivity is in the order of 100 μΩ cm, so called "bad" metals, $CoSn_2$ possesses a significantly lower resistivity. A comparison of the values measured for $FeSn_2$ and $CoSn_2$ with published values ($\rho_{293} = 170$ μΩ m[61] and $\rho_{293} =$

Table 2. Crystallographic data for $MnSn_2$, $FeSn_2$ and $CoSn_2$ after annealing at 150 °C.

	$MnSn_2$	$FeSn_2$	$CoSn_2$
crystal size [mm^3]	$0.12\times0.14\times0.22$	$0.06\times0.06\times0.20$	$0.06\times0.05\times0.05$
a [Å]	6.671(2)	6.545(2)	6.373(3)
c [Å]	5.443(3)	5.326(4)	5.463(4)
V [$Å^3$]	242.2(2)	228.2(2)	221.9(2)
ρ_{calcd} [$g\,cm^{-3}$]	8.017	8.537	8.870
space group	*I*4/*mcm*	*I*4/*mcm*	*I*4/*mcm*
μ [mm^{-1}]	25.170	27.542	29.260
$F(000)$	500	504	508
2θ range [°]	4.32–69.76	4.40–69.86	4.52–69.55
hkl indices	$-13\le h\le14$	$-14\le h\le8$	$-16\le h\le14$
	$-16\le k\le16$	$-17\le k\le15$	$-15\le k\le12$
	$-14\le l\le7$	$-7\le l\le13$	$-8\le l\le12$
reflns	3121	2881	3026
independent reflns	630	558	570
parameters	8	8	8
goodness-of-fit	1.190	1.257	1.110
R_1/wR_2 [$I_0>2\sigma(I_0)$]	0.036/0.088	0.038/0.095	0.037/0.089
R_1; wR_2 (all)	0.038/0.094	0.040/0.097	0.047/0.095
extinction coefficient	0.109(5)	0.035(3)	0.016(2)
$\Delta\rho_{min}/\Delta\rho_{max}$ [$Å^{-3}$]	−4.022/5.068	−3.683/10.637	−4.617/3.175
Atomic parameters[a]	$MnSn_2$	$FeSn_2$	$CoSn_2$
T in 4*a* (0, 0, $^1/_4$)			
U_{eq} [10^{-4} Å]	53.5(8)	50.3(8)	77(1)
U_{11} [10^{-4} Å]	48.1(9)	38(1)	72(2)
U_{33} [10^{-4} Å]	64(1)	74(2)	86(4)
Sn in 8*h* (x, $x+{}^1/_2$, 0)	$x=0.16156(2)$	$x=0.16112(3)$	$x=0.16491(4)$
U_{eq} [10^{-4} Å]	71.1(6)	55.5(7)	62.8(8)
U_{11} [10^{-4} Å]	58.1(7)	45.1(8)	54.8(8)
U_{33} [10^{-4} Å]	97.1(9)	76(1)	79(1)
U_{12} [10^{-4} Å]	−13.2(3)	−6.7(5)	−5.4(7)

[a] For site 4*a* $U_{22}=U_{11}$, $U_{ij}=0$, for site 8*h* $U_{22}=U_{11}$ and $U_{13}=U_{23}=0$.

52 μΩ m[61]) shows only small differences that can be attributed to the use of single crystalline samples in our case. $MnSn_2$ has been described as semiconductor ($\rho_{293}=$ 110 μΩ m[61]) as well as metal ($\rho_{280}=195$ μΩ m[49]). Our measurements on non-oxidised samples confirm the metal-like behaviour, which is in agreement with the quantum-chemical band structure calculations (see below). The differences in the literature can be assigned to partially decomposed samples, since these are air sensitive and were not handled in inert atmosphere. By applying the one-band approximation, the charge carrier concentration can be estimated. The carrier concentration decreases in the sequence $CoSn_2$ (R_{132}: 2 e^-; R_{213}: 81 e^-) > $MnSn_2$ (R_{132}: 20 e^-; R_{213}: 10 e^-) > $FeSn_2$ (R_{132}: 1 e^-). In all three compounds, electrons are the dominating carriers. In comparison to $CoSn_2$, $MnSn_2$ shows only a small anisotropy. The Hall measurement on $FeSn_2$ reveals a strong temperature dependence which indicates bands with different character and different mobility.

Quantum chemical calculations: Figure 3 displays the electronic densities of states of the TSn_2 compounds. For compatibility, the density of states (DOS) is shown without separating the different spin contributions in $MnSn_2$ and $FeSn_2$. While the DOS in $CoSn_2$ and $MnSn_2$ shows no minimum at the Fermi energy a pseudo gap is revealed for $FeSn_2$.

In all compounds, several bands are crossing the Fermi energy, thus accounting for the observed metallic behaviour of the electrical resistivity. Magnetic moments of 2.83 and 1.63 μ_B are calculated for $MnSn_2$ and $FeSn_2$, respectively. These values are in excellent agreement with the reported values of 2.36–3.11 μ_B for $MnSn_2$[62] and 1.64 μ_B for $FeSn_2$[63].

The electron localisability indicator (ELI) is representatively displayed for $CoSn_2$ in Figure 4. Four different attractor types are found for all three compounds. Two of the attractor types are homoatomic and two are heteroatomic. The two attractors involving tin atoms—A with a disynaptic basin V^2(Sn, Sn), denoted as Ω_A, on the Sn–Sn contact *d*1 and B with a tetrasynaptic basin V^4(Sn, Sn, T, T) on *d*2 (Ω_B)—reveal the bonds connecting the tin atoms to the interpenetrating 6^3 nets. The transition metal atoms are forming chains parallel to [001] by the bonds with the basin V^2(T, T) on *d*6 (Ω_D). In addition, the structuring of the ELI in the third shell of the transition metal atoms indicates a participation of their d electrons in the bonding.[64] The chains are connected to the interpenetrating Sn 6^3 nets by the attractor C with the trisynaptic basin V^3(T, Sn, T), centred in the triangle of the distances *d*5–*d*6–*d*5 (Ω_C) resulting in a three-dimensional network. In Table 3 the electron counts for the different basins are listed. The electron population in the Ω_A basin is increasing with increasing atomic number, reaching a value of 1.9 in $CoSn_2$. This interaction may be un-

Table 3. Populations of the ELI basins in TSn_2 (T = Mn, Fe, Co).

		Basin	n [e]
$MnSn_2$	Ω_A	V^2(Sn, Sn)	1.6
	Ω_B	V^4(Sn, Sn, Mn, Mn)	1.2
	Ω_C	V^3(Mn, Sn, Mn)	1.5
	Ω_D	V^2(Mn, Mn)	0.1
$FeSn_2$	Ω_A	V^2(Sn, Sn)	1.8
	Ω_B	V^4(Sn, Sn, Fe, Fe)	1.7
	Ω_C	V^3(Fe, Sn, Fe)	1.2
	Ω_D	V^2(Fe, Fe)	<0.1
$CoSn_2$	Ω_A	V^2(Sn, Sn)	1.9
	Ω_B	V^4(Sn, Sn, Co, Co)	1.7
	Ω_C	V^3(Co, Sn, Co)	1.1
	Ω_D	V^2(Co, Co)	0.1

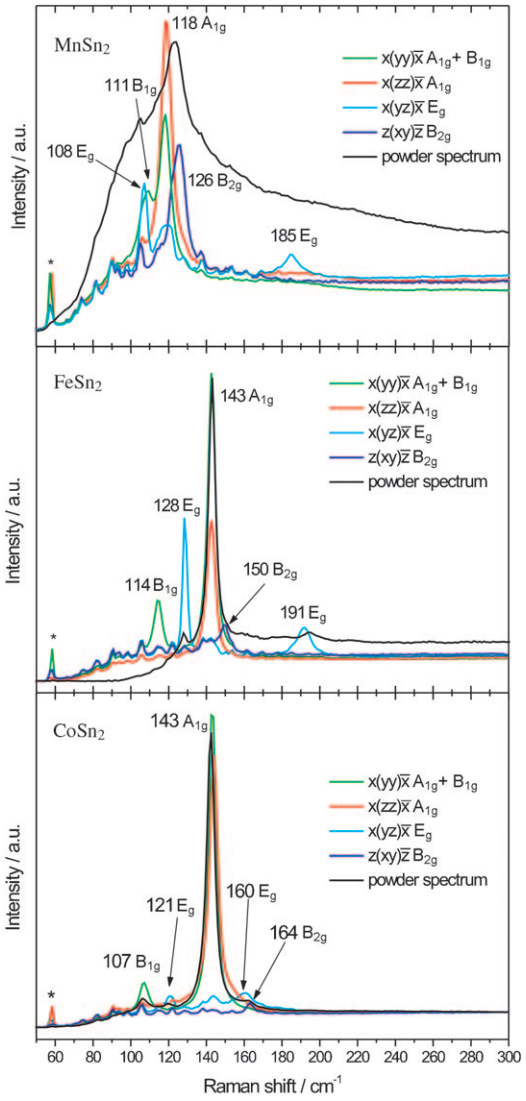

Figure 1. Raman spectra of $MnSn_2$, $FeSn_2$ and $CoSn_2$. The spectra are labelled according to Porto.[60]

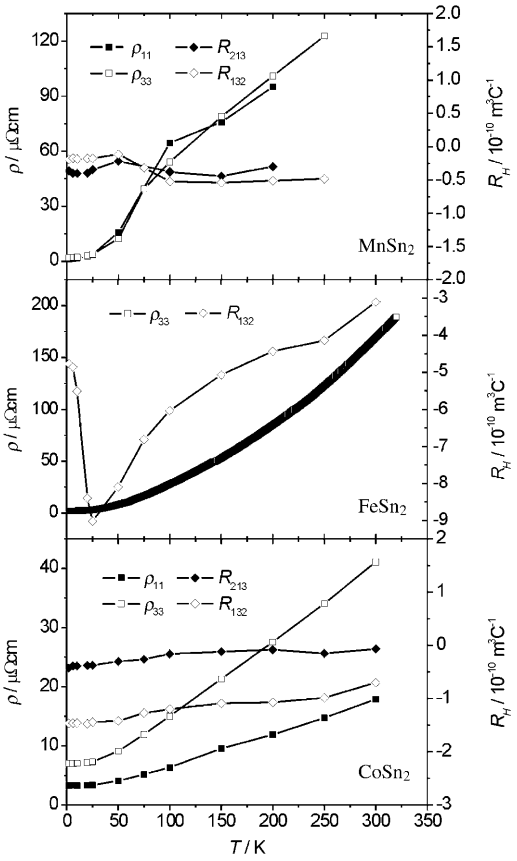

Figure 2. Temperature dependence of the Hall effect (R_{213} and R_{132}) and resistivity (ρ_{11} and ρ_{33}) tensors for TSn_2 (T = Mn, Fe, Co).

derstood as a two-centre two-electron bond. The trend in the tetrasynaptic basins Ω_B is similar, but their populations are lower than those of Ω_A. In the trisynaptic basins Ω_C the population is decreasing by going from $MnSn_2$ to $CoSn_2$. The disynaptic basin Ω_D has only a tiny population.

The ELI values of the attractors as well as of the interconnecting points, where the basins grow together, can be combined in bifurcation diagrams.[65] This representation reveals topological similarities of the ELI in different compounds. The bifurcation diagrams for TSn_2 (T = Mn, Co, Fe) clearly show their identical bonding behaviour (Figure 5).

Bond order: Table 4 is summarising the relevant distances *d*1 to *d*6 in the compounds with the according Pauling bond orders (PBO) *n* [Eq. (1)].

$$D(n) = D(1) - 0.60\log(n) \qquad (1)$$

Table 4. Distances and according Pauling bond orders (PBOs) in the compounds $MnSn_2$, $FeSn_2$ and $CoSn_2$.

	$MnSn_2$		$FeSn_2$		$CoSn_2$	
	Length [Å]	PBO	Length [Å]	PBO	Length [Å]	PBO
*d*1(Sn–Sn)	3.042	0.40	2.977	0.51	2.968	0.52
*d*2(Sn–Sn)	3.191	0.22	3.126	0.29	3.129	0.28
*d*3(Sn–Sn)	3.468	0.08	3.392	0.10	3.443	0.08
*d*4(Sn–Sn)	3.534	0.06	3.467	0.08	3.360	0.12
*d*5(T–Sn)	2.845	0.35	2.789	0.43	2.740	0.50
*d*6(T–T)	2.720	0.23	2.660	0.29	2.729	0.21

For the calculation, single-bond radii of 1.17 Å for Mn and Fe were employed, while 1.16 and 1.40 Å were used for Co and Sn, respectively.[66] From the evaluated PBOs one would expect significant bonding interactions on the distances *d*1, *d*2, *d*5 and *d*6. This is in accordance with the ELI calculations apart from *d*5, for which the PBO, by definition, can only indicate two-centre interactions but the ELI reveals three-centre interactions.

A more comprehensive characterisation of the bonding can be gained by fitting an harmonic force-constant model—based on the key atomic interactions as revealed by the ELI calculation—to the experimentally observed Raman frequencies. Since the number of available data is restricted (all efforts to measure the infrared active modes in transmis-

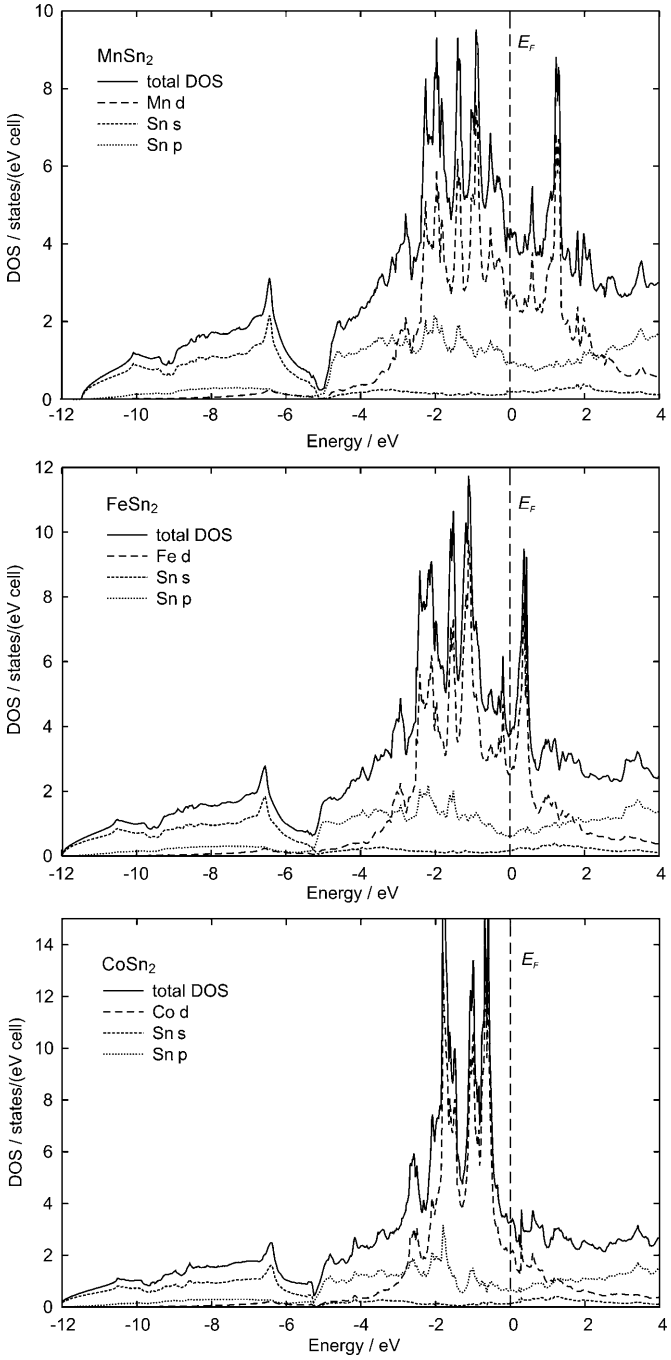

Figure 3. Electronic density of states for $MnSn_2$, $FeSn_2$ and $CoSn_2$. In all compounds several bands are crossing the Fermi level, reflecting the metallic behaviour.

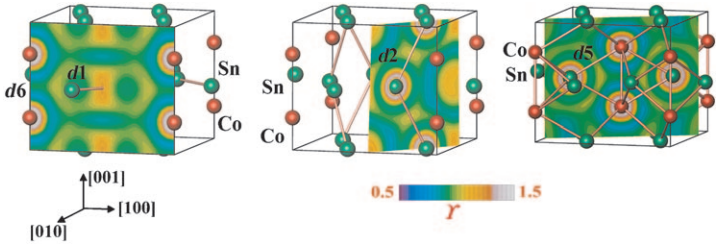

Figure 4. ELI diagrams of $CoSn_2$. The slices cut the named distances in the middle, thus revealing the interactions between the atoms.

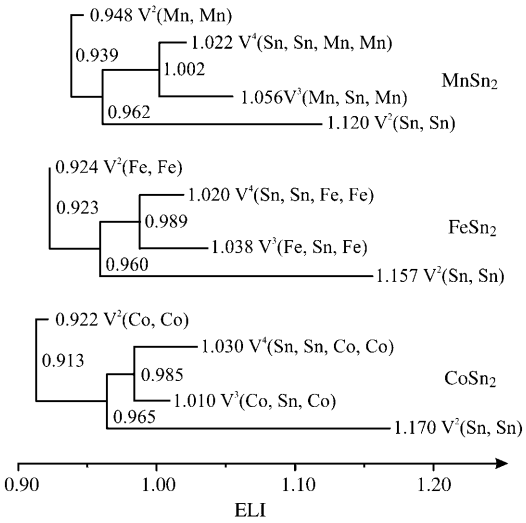

Figure 5. Bifurcation diagrams for $MnSn_2$, $FeSn_2$ and $CoSn_2$, showing the identical bonding topology revealed by the ELI calculations.

sion or reflection failed) the model has to be simple. One longitudinal force constant was ascribed to *d*1, another one to *d*2, thus resembling the interactions in the Sn 6^3 nets. As in the case of the isostructural compounds investigated earlier, the three-centre bond is described by a longitudinal and a transversal force constant on the *d*5 interaction. From the Raman measurements no statement can be made concerning the strength of the interaction between the T atoms (*d*6 interaction), since no longitudinal movement of them is involved in the Raman active modes (for details see references [30,38]). The force-constant model was developed within the programmes Vibratz[67] and Unisoft[68,69] and fitted to the experimental data. The stability of the model was ensured by absence of phonon branches with zero energy in the phonon dispersion. The retrieved force constants are given in Table 5, while the calculated and measured frequencies are opposed in Table 6.

Table 5. Force constants [in Ncm^{-1}] retrieved from the Raman spectroscopic data.

Interaction	$MnSn_2$	$FeSn_2$	$CoSn_2$
*d*1	0.293	0.426	0.590
*d*2	0.315	0.482	0.401
*d*5 longitudinal	0.300	0.312	0.239
*d*5 transversal	0.005	0.007	0.005

Table 6. Measured and calculated Raman frequencies [in cm^{-1}].

	$MnSn_2$		$FeSn_2$		$CoSn_2$	
	Exptl	Calcd	Exptl	Calcd	Exptl	Calcd
A_{1g}	118	122	143	147	143	153
B_{1g}	111	109	114	111	107	115
B_{2g}	126	122	150	147	164	170
E_g	108	108	128	129	121	96
E_g	185	186	191	194	160	153

For $MnSn_2$ and $FeSn_2$ the measured and calculated frequencies agree within the experimental error (average deviations are 1.4 and 1.5 cm^{-1}, respectively), while the difference is larger in the case of $CoSn_2$ (average deviation 4.9 cm^{-1}).

To compare the empirical bond orders derived by Pauling's method with the experimentally determined force constants, an experimental bond order has to be established. The spectroscopically determined force constants for the formal Sn–Sn single bonds in $(CH_3)_3Sn–Sn(CH_3)_3$ and $(C_6H_5)_3Sn–Sn(C_6H_5)_3$ are 1.2 and 1.4 $N\,cm^{-1}$, respectively.[70,71] Comparisons of these values with the force constants of *d*1 and *d*2 reveal bond orders between 0.2 and 0.5, that is, significantly lower than 1, in agreement with the calculated PBOs.

A force constant for a formal Mn–Sn single bond can be derived from $(CO)_5Mn–Sn(CH_3)_3$.[72] From a frequency of 178 cm^{-1}, a force constant of 0.7 $N\,cm^{-1}$ is calculated within the harmonic approximation neglecting non-metallic atoms. This results in an experimental bond order of 0.86 (two longitudinal force constants on *d*5 give one three-centre interaction) for the Mn–Sn–Mn bonds. For a Fe–Sn interaction, the only spectroscopic data available is for $(\pi\text{-}C_5H_5)(CO)_2Fe–SnCl_3$.[73] From the vibrational frequency of 222 cm^{-1}, a force constant of 1.1 $N\,cm^{-1}$ is derived. To be consistent with the value for the Mn–Sn interaction, the influence of the chlorine substituents has to be taken into account. The effect can be seen by comparing the bond strengths of the Co–Sn bonds in the series $(CO)_4Co–Sn(CH_3)_3$, $(CO)_4Co–SnBr_3$ and $(CO)_4Co–SnCl_3$. From the force constants of 0.72, 1.05 and 1.23 $N\,cm^{-1}$, respectivelym follows a correction of −0.51 $N\,cm^{-1}$ for the Fe–Sn interaction, resulting in the strength of a single bond for the Fe-Sn-Fe interaction. For the Co–Sn–Co interactions, an experimental bond order of 0.7 is calculated.

Chemical bonding: According to our investigations, a consistent bonding model describing the chemical bonding in the compounds $MnSn_2$, $FeSn_2$ and $CoSn_2$ can be derived. The ELI calculations reveal four different interactions in the compounds. The tin atoms are forming interpenetrating 6^3 nets by homoatomic interactions along *d*1 and *d*2. From the quantum-chemical calculations the bonds on *d*1 can be described as two-centre two-electron bonds, while the four-centre bonds along *d*2 have a lower electron count. This difference in electron counts of *d*1 and *d*2 is not displayed in the bond strengths, determined by Raman measurements. The T atoms form chains parallel to [001] (ELI attractor on *d*6). The chains and the interpenetrating 6^3 nets are connected by three-centre T–Sn–T bonds (*d*5). Figure 6 displays the general bonding situation in the TSn_2 compounds.

In contrast to the model suggested by Nowotny and Schubert,[37] who also proposed Sn 6^3 nets and T chains, the interactions between these building groups are not ionic, but covalent as shown by the ELI.

From a comparison of the six isostructural compounds investigated by the methodology used herein, it can be concluded, that the chemical bonding in these intermetallic compounds of the $CuAl_2$ family depends on the main-group metal. In $CuAl_2$[30,38] and the stannides $MnSn_2$, $FeSn_2$ and $CoSn_2$ the main-group metals form interpenetrating 6^3 nets, while only Sb_2 dumbbells are formed in the antimonides $TiSb_2$ and VSb_2.[30,39] In addition, the transition-metal atoms in the stannides and antimonides form chains along [001]. This interaction is absent in $CuAl_2$. The homoatomic building groups in the compounds are connected by three-centre bonds resulting in a three-dimensional network in all cases. The difference in the bonding situation is not only shown in the Raman spectra and the resulting bond orders, but also in the pressure dependence of the *c*/*a* ratio (Figure 7).

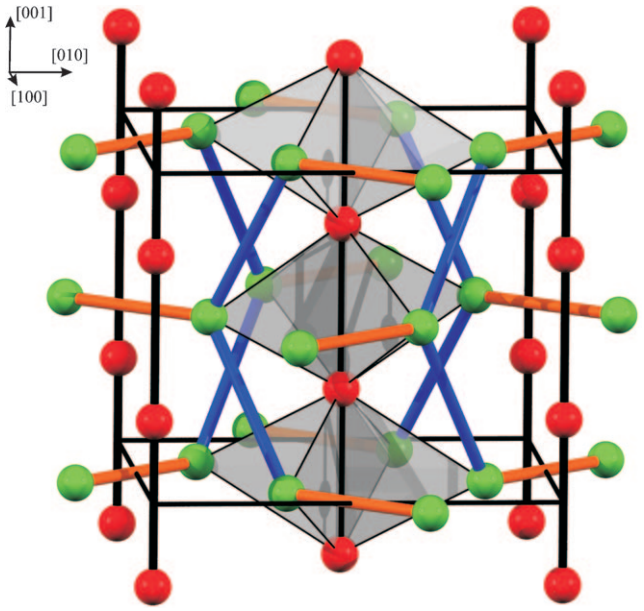

Figure 6. Representation of the chemical bonding in $MnSn_2$, $FeSn_2$ and $CoSn_2$ (T = red, Sn = green). Bonds along *d*1 are orange, while bonds along *d*2 are blue. The three-centre bonds (grey triangles) are only shown for the central chain.

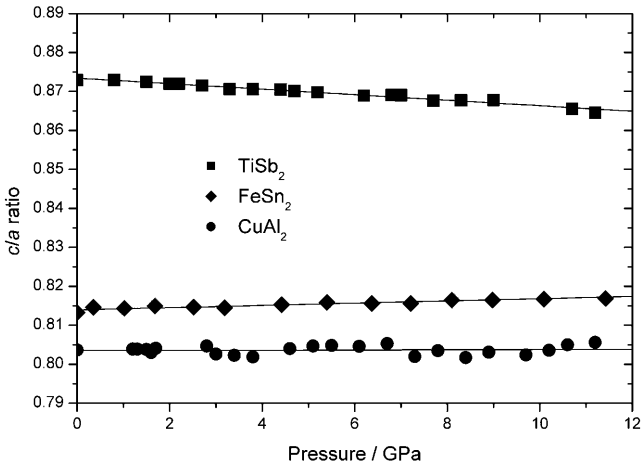

Figure 7. Pressure dependence of the *c*/*a* ratio of $TiSb_2$,[39] $FeSn_2$[74] and $CuAl_2$[38] indicating different bonding situations in the class of compounds.

While in $TiSb_2$ it is decreasing with increasing pressure, due to the absence of the *d*2 bond, it is constant in $CuAl_2$. In $FeSn_2$ the *c*/*a* ratio is increasing with pressure[74,75] which results from the additional gained stiffness along [001] due to the presence of the Fe-Fe interaction detected by the ELI calculations.

Conclusion

The compounds $MnSn_2$, $FeSn_2$ and $CoSn_2$ are line compounds, which decompose peritectically at 555, 531, and 556 °C, respectively. The chemical bonding in the compounds is described as interpenetrating 6^3 nets formed by homoatomic Sn interactions along *d*1 and *d*2 contacts. The T atoms (T = Mn, Fe or Co) are building chains parallel to [001]. Both structural units are connected through three-centre T–Sn–T bonds. In addition to these covalent interactions, the electrical conductivities of these materials show metal-like temperature dependence. The developed bonding model is physically meaningful as supported by Raman and Mößbauer spectroscopy and reflected in the pressure dependence of the *c*/*a* ratio. Comparison with other isostructural compounds of the $CuAl_2$ family reveals the dependence of the connectivity pattern on the main group metal.

Experimental Section

Preparation: Single-phase and two-phase polycrystalline samples of $MnSn_2$ and $CoSn_2$ were prepared in an argon-filled glove-box (O_2 and H_2O below 1 ppm) by mixing and pressing pellets of appropriate amounts of the elements (Mn: powder, ChemPur 99.99%; Co: powder, Merck; Sn: bar, ChemPur 99.999%), which were then molten several times in an arc melter (Centorr Vacuum Industries, Model 5BJ, 50 A, 72 V) on a water cooled copper hearth under a protective atmosphere of Ti-gettered argon. A weight loss between 0.1 and 0.5 wt.% was observed. To obtain thermodynamic equilibrium the ingots were annealed in evacuated quartz glass ampoules for 14 days at 500 °C and subsequently quenched in water.

Fe-Sn samples were prepared by pressing pellets of the necessary amounts of Fe (powder, ChemPur 99.99+%) and Sn in a glove-box and enclosing the pellets in evacuated quartz glass ampoules. After a heat treatment at 500 °C for 40 days, equilibrated single- and two-phase samples were obtained.

Large single crystals up to several mm of $MnSn_2$ [and $CoSn_2$] could be obtained by melting the compounds in evacuated quartz glass ampoules with excess tin (ratio TSn_2:Sn = 1:3.6 [1:30]) at 900 °C [700 °C] and homogenising the melt for 24 h. After cooling the melt in 2 h to 450 °C [500 °C] the temperature was held constant for 24 h before increasing the temperature to 600 °C in 4 h for both compounds. In the last step, the melt was cooled to ambient temperature in 240 h. In the case of $CoSn_2$, the melt was cooled to 350 °C and subsequently quenched in water to ambient temperature to avoid the formation of $CoSn_3$.[57]

Single crystals of $FeSn_2$ were also synthesised from the Sn flux ($FeSn_2$:Sn = 1:10) by heating the mixture in evacuated quartz glass ampoules to 500 °C in 24 h, holding the temperature for 24 h and cooling the melt down to ambient temperature in 240 h.

To isolate the crystals from the ingots, the β/α-phase transition of Sn at 13.2 °C was exploited.[76] The ingots were inoculated with small α-Sn crystals and then stored at −78.5 °C for 7 to 12 d. The phase transition results in a volume increase of 26%, thus breaking up the Sn matrix and releasing the well-shaped single crystals of the stannides without damage or destruction of the surface.

Since $MnSn_2$ is not air stable, the Mn–Sn samples were handled and stored in inert argon atmosphere.

X-ray diffraction: X-ray powder diffraction experiments were performed on a Guinier image plate camera Huber G670 with $Cu_{K\alpha1}$ radiation (SiO_2 monochromator, $\lambda_{Cu} = 1.540562$ Å) by using Ge as internal standard ($a = 5.65752$ Å). The samples were finely ground and spread on a 6 μm thick Mylar foil (Chemplex) coated with Vaseline. Lattice parameters were refined on definite sets of 11, 12 and 14 reflections for $MnSn_2$, $FeSn_2$ and $CoSn_2$, respectively, with the program WinCSD.[77]

Single-crystal structure determination of the compounds was performed on an R-AXIS RAPID diffractometer (Rigaku/MSC). The diffractometer was equipped with a graphite monochromator and a Mo X-ray source ($\lambda_{Mo} = 0.71073$ Å, 50 kV, 40 mA). After numerical absorption correction, the crystal structure was solved and refined against F^2 by using the SHELX-97[78,79] software as implemented in the WinGX[80] programme package.

EDXS and WDXS measurements: Pieces of the ingots or single crystals were embedded in Polyfast (Struers), metallographically polished and then investigated with a SEM (XL 30, Phillips, 25 kV) equipped with LaB_6 filament and Si(Li) detector to detect impurities. WDXS analyses were carried out with a SX 100 at 25 kV (Cameca) to determine the exact composition with the pure elements as standards.

DSC measurements: Samples were measured in a STA 409 PC on a DSC/TG HIGH RG 2 measuring head (Netzsch) with a heating rate of 10 K min^{-1}. The transition temperatures were determined from the onset of the signals and given temperatures are accurate within 2 °C.

Chemical analysis: Nitrogen and oxygen contents were determined using three samples, each of 50 to 60 mg mass, for every compound by the carrier gas-hot-extraction method in a TC-436 DR (LECO), while the transition metal and tin content were determined by inductively-coupled plasma mass spectrometry (ICP-MS) in a PQ ExCell (TJA).

Density measurements: He-gas-pycnometric density measurements were performed on a sample of several $FeSn_2$ crystals in an AccuPyc 1330 (Micromeritics). Prior to the measurements the sample chamber was flushed several times with helium. The given value is the average of 25 measurements.

Raman spectroscopy: To obtain spectra of powdered samples, finely ground single crystals were pressed into a thin pellet to ensure sufficient thermal conductivity. Single crystals were mounted on a goniometer head and aligned with a precision higher than 0.3° by means of Weissenberg and Laue techniques (Huber, Weissenberg Goniometer 102 and Stoe, Lattice Explorer, respectively). A specially constructed adapter was used to attach the adjusted goniometer head to the Raman spectrometer (Labram 010, JobinYvon) without altering the orientation.

The Raman measurements were performed in backscattering geometry and two notch filters for low-frequency performance allowed for the recognition of modes with small Raman shifts (> 70 cm^{-1}). To avoid decomposition of the samples, the laser beam had to be attenuated by a factor of ten before the sample. Exposures of 100 to 5000 s were conducted using an auto-focus system. Twenty measurements were averaged to increase the signal-to-noise ratio. As excitation source, a He/Ne or an Ar laser, operating at 633 nm (15 mW) and 488 nm (50 mW), respectively, were used. The spectral width of the spectra is about 4 cm^{-1} and polarised spectra are labelled according to Porto.[60]

Hall-tensor components and electrical conductivity: Two single crystalline slabs of each compound were employed to measure the two independent components of the Hall tensor, for details see references [30,38,39]. Electrical contacts (wire: Cu 50 μm or Pt 30 μm) were fixed with silver-containing epoxy resin (Epotek H20E) hardened at 150 °C. The samples were transferred to a magnet cryostat (MPMS XL7), connected to a DC current source (Keithley 224) and a nanovoltmeter (34420 A, Hewlett–Packard). An isothermal series was recorded after thermal equilibration while sweeping the magnetic field from 5 T to −5 T and back to zero. The labeling of the different tensor components follows the recommendation of Haussühl.[59]

Quantum chemical calculations: Spin-polarised electronic structure calculations, including band structure, density of states (DOS) and electron localisability indicator (ELI[81] evaluated in the ELI-D representation according to[82,83]), were performed with the TB-LMTO-ASA programme package.[84] The structural parameters for $FeSn_2$ and $CoSn_2$ were taken from the experimentally determined structures,[31] while for $MnSn_2$ the values in the current work form the basis of the calculations.

The calculations were performed spin-polarised for all three compounds, confirming the magnetic behaviour for $MnSn_2$ and $FeSn_2$ and showing no magnetic moment for $CoSn_2$. A basis set containing T(4s, 4p, 3d) and Sn(5s, 5p) states were used for self-consistent calculations with Sn(5d, 4f) states being downfolded.[85] Due to the small overlap of the atomic spheres, no empty spheres had to be added in the calculations (r_{Mn} = 1.588 and r_{Sn} = 1.735 Å; r_{Fe} = 1.551 and r_{Sn} = 1.703 Å; r_{Co} = 1.523 and r_{Sn} = 1.693 Å). The ELI was calculated on an adequately fine mesh of 0.03 Å. Determination of the critical points, evaluation of basins and the integration of the electron density inside these were performed numerically with the program Basin.[86]

Acknowledgements

We acknowledge G. Auffermann and R. Niewa for performing chemical analyses and DSC investigations, respectively, and F. R. Wagner for his assistance with the quantum chemical calculations. We thank R. Ramlau for WDXS investigations. U. Burkhardt is acknowledged for the metallographic preparations.

[1] O. Nial, *Z. Allg. Anorg. Chem.* **1938**, *238*, 287–296.
[2] O. Nial, *Ark. Kemi Mineral. Geol. B* **1943**, *17*, No. 11.
[3] W. F. Ehret, A. F. Westgren, *J. Am. Chem. Soc.* **1933**, *55*, 1339–1351.
[4] C. Noeller, *Justus Liebigs Ann. Chem.* **1860**, *115*, 233–237.
[5] A. S. Russell, T. R. Kennedy, R. P. Lawrence, *J. Chem. Soc.* **1934**, 1750–1754.
[6] F. Stromberg, V. E. Kuncser, K. Westerholt, W. Keune, *Phys. Status Solidi C* **2004**, *1*, 3754–3759.
[7] R. A. Dunlap, S. W. Kehoe, J. R. Dahn, J. W. O'Brian, *J. All. Compd.* **2005**, *400*, 252–256.
[8] H. Guo, H. Zhao, X. Jia, X. Li, W. Qiu, *Electrochim. Acta* **2007**, *52*, 4853–4857.
[9] J.-J. Zhang, Y.-Y. Xia, *J. Electrochem. Soc.* **2006**, *153*, A1466–A1471.
[10] M.-Z. Xue, Z.-W. Fu, *Solid State Ionics* **2006**, *177*, 1501–1507.
[11] C. M. Ionica-Bousquet, P. E. Lippens, L. Aldon, J. Olivier-Fourcade, J.-C. Jumas, *Chem. Mater.* **2006**, *18*, 6442–6447.
[12] R. A. Covert, H. H. Uhlig, *J. Electrochem. Soc.* **1957**, *104*, 537–542.
[13] N. Sarafianos, *Mater. Sci. Technol.* **1987**, *3*, 66–71.
[14] J. Osswald, R. Giedigkeit, R. E. Jentoft, M. Armbrüster, F. Girgsdies, K. Kovnir, Y. Grin, R. Schlögl, T. Ressler, *J. Catal.* **2008**, *258*, 210–218.
[15] K. Kovnir, M. Armbrüster, D. Teschner, T. V. Venkov, F. C. Jentoft, A. Knop-Gericke, Yu. Grin, R. Schlögl, *Sci. Technol. Adv. Mater.* **2007**, *8*, 420–427.
[16] W. Klemm, *Proc. Chem. Soc. London* **1958**, 329–341.
[17] W. Klemm, E. Busmann, *Z. Allg. Anorg. Chem.* **1963**, *319*, 297–311.
[18] F. Laves, *Naturwissenschaften* **1941**, *29*, 244–255.
[19] E. Zintl, *Naturwissenschaften* **1929**, *17*, 782–783.
[20] E. Zintl, W. Dullenkopf, *Z. Phys. Chem. Abt. B* **1932**, *16*, 195–205.
[21] E. Zintl, G. Brauer, *Z. Phys. Chem. Abt. B* **1933**, *20*, 245–271.
[22] W. Hume-Rothery, *J. Inst. Met.* **1926**, *25*, 295–361.
[23] A. F. Westgren, G. Phragmén, *Ark. Mat. Astron. Fys.* **1926**, *19*, No. 12.
[24] A. F. Westgren, G. Phragmén, *Z. Metallkd.* **1926**, *18*, 279–284.
[25] A. F. Westgren, G. Phragmén, *Trans. Faraday Soc.* **1929**, *25*, 379–385.
[26] W. Ekman, *Z. Phys. Chem. Abt. B* **1931**, *12*, 57–78.
[27] F. Laves, H. Witte, *Metallwirtschaft* **1936**, *15*, 840–842.
[28] F. Laves, *Naturwissenschaften* **1939**, *27*, 65–73.
[29] E. Zintl, A. Harder, *Z. Phys. Chem. Abt. B* **1932**, *16*, 206–212.
[30] M. Armbrüster, *Bindungsmodelle für intermetallische Verbindungen mit der Struktur des $CuAl_2$-Typs*, Cuvillier, Göttingen, **2005**.
[31] M. Armbrüster, M. Schmidt, R. Cardoso Gil, H. Borrmann, Yu. Grin, *Z. Kristallogr.* **2007**, *222*, 83–84.
[32] Y. Dong, F. J. DiSalvo, *Acta Crystallogr. Sect. E* **2005**, *61*, i282-i284.
[33] U. Häusermann, S. Lidin, *J. Solid State Chem.* **1997**, *132*, 151–155.
[34] U. Häusermann, S. Lidin, *J. Solid State Chem.* **1997**, *134*, 431.
[35] K. Schubert, *Kristallstrukturen zweikomponentiger Phasen*, Springer, Berlin, **1964**.
[36] W. B. Pearson, *The Crystal Chemistry and Physics of Metals and Alloys*, Wiley Interscience, New York, **1972**.
[37] H. Nowotny, K. Schubert, *Z. Metallkd.* **1946**, *37*, 17–23.
[38] Y. Grin, F. R. Wagner, M. Armbrüster, M. Kohout, A. Leithe-Jasper, U. Schwarz, U. Wedig, H. G. von Schnering, *J. Solid State Chem.* **2006**, *179*, 1707–1719.
[39] M. Armbrüster, W. Schnelle, U. Schwarz, Y. Grin, *Inorg. Chem.* **2007**, *46*, 6319–6328.
[40] M. A. Abidov, R. N. Kuz'min, S. V. Nikitina, *J. Exp. Theor. Phys.* **1969**, *29*, 957–1189.
[41] G. Fabri, E. Germagnoli, M. Musci, G. C. Locati, *Nuovo Cimento B* **1965**, *40*, 178–183.
[42] V. A. Golovnin, S. B. Zezin, R. N. Kuz'min, *Sov. Phys. Sol. State* **1972**, *14*, 1313–1315.
[43] G. Le Caër, B. Malaman, G. Venturini, D. Fruchart, B. Roques, *J. Phys. F* **1985**, *15*, 1813–1827.
[44] V. I. Nikolaev, V. S. Rusakov, *Sov. Phys. Sol. State* **1975**, *17*, 200–201.
[45] A. M. Van der Kraan, K. H. J. Buschow, *Physica B+C* **1986**, *138*, 55–62.
[46] G. Venturini, B. Malaman, G. Le Caër, D. Fruchart, *Phys. Rev. B* **1987**, *35*, 7038–7045.
[47] M. Armbrüster, P. Simon, Yu. Grin, *Z. Allg. Anorg. Chem.* **2004**, *630*, 1702.
[48] K. Chen, G. D. Wilcox, *Phys. Rev. Lett.* **2005**, *94*, 066104/1.
[49] J. S. Kouvel, C. C. Hartelius, *Phys. Rev.* **1961**, *123*, 124–125.
[50] G. Le Caër, B. Malaman, G. Venturini, I. B. Kim, *Phys. Rev. B* **1982**, *26*, 5085–5096.
[51] K. Yasukochi, K. Kanematsu, T. Ohoyama, *J. Phys. Soc. Jpn.* **1961**, *16*, 1123–1130.
[52] E. Wachtel, R. Ulrich, *Z. Metallkd.* **1968**, *59*, 227–236.
[53] F. Wever, W. Reinecken, *Z. Allg. Anorg. Chem.* **1926**, *151*, 349–372.
[54] C. A. Edwards, A. Preece, *J. Iron Steel Inst. London* **1931**, *124*, 41–69.
[55] K. Lewkonja, *Z. Allg. Anorg. Chem.* **1908**, *59*, 293–345.
[56] S. F. Zemczuzny, S. W. Belynsky, *Z. Allg. Anorg. Chem.* **1908**, *59*, 364–370.
[57] A. Lang, W. Jeitschko, *Z. Metallkd.* **1996**, *87*, 759–764.
[58] L. A. Panteleimonov, G. F. Portnova, O. P. Nesterova, *Moscow Univ. Chem. Bull. (Engl. Transl.)* **1971**, *26*, 79–80.
[59] S. Haussühl, *Kristallphysik*, Leipzig, Deutscher Verlag für Grundstoffindustrie, **1983**.
[60] T. C. Damen, S. P. S. Porto, B. Tell, *Phys. Rev.* **1966**, *142*, 570–574.
[61] L. D. Dudkin, V. I. Vaidanich, *Sov. Phys. Sol. State* **1960**, *2*, 377–378.
[62] L. M. Corliss, J. M. Hastings, *J. Appl. Phys.* **1963**, *34*, 1192.
[63] G. Venturini, D. Fruchart, J. Hübsch, G. Le Caër, B. Malaman, B. Roques, *J. Phys. F* **1985**, *15*, 427–438.
[64] M. Kohout, F. R. Wagner, Yu. Grin, *Theo. Chem. Acc.* **2002**, *108*, 150–156.
[65] A. Savin, B. Silvi, F. Colonna, *Can. J. Chem.* **1996**, *74*, 1088–1096.
[66] L. Pauling. *The Nature of the Chemical Bond and the Structure of Molecules and Crystals*, Cornell University Press, Ithaca, **1960**.
[67] VIBRATZ Version 1.2, E. Dowty, Shape Software, **2002**.
[68] G. Eckold, M. Stein-Arsic, H. J. Weber, *J. Appl. Crystallogr.* **1987**, *20*, 134–139.
[69] P. Elter, G. Eckold, *Physica B+C* **2000**, *276–278*, 268–269.
[70] P. A. Bulliner, C. O. Quicksall, T. G. Spiro, *Inorg. Chem.* **1971**, *10*, 13–18.

[71] B. Fontal, T. G. Spiro, *Inorg. Chem.* **1971**, *10*, 9–13.
[72] R. A. Burnham, S. R. Stobart, *J. Chem. Soc. Dalton* **1973**, 1269–1274.
[73] S. R. A. Bird, J. D. Donaldson, A. F. L. C. Holding, B. C. Senior, M. J. Tricker, *J. Chem. Soc. A* **1971**, 1616–1621.
[74] H. Giefers, M. Nicol, *J. Alloys Compd.* **2006**, *422*, 132–144.
[75] H. Giefers, M. Nicol, *J. Phys. Chem. Solids* **2006**, *67*, 2027–2032.
[76] E. Cohen, A. K. W. A. van Lieshout, *Z. Phys. Chem. Abt. A* **1935**, *173*, 32–34.
[77] L. G. Akselrud, P. Yu. Zavalij, Yu. Grin, V. K. Pecharsky, B. Baumgartner, E. Wölfel, *Mater. Sci. Forum* **1993**, *133–136*, 335–340.
[78] SHELXS-97, Release 97-2, G. M. Sheldrick, **1997**.
[79] SHELXL-97, Release 97-2, G. M. Sheldrick, **1997**.
[80] L. J. Farrugia, *J. Appl. Crystallogr.* **1999**, *32*, 837–838.
[81] M. Kohout, *Int. J. Quantum Chem.* **2004**, *97*, 651–658.
[82] M. Kohout, F. R. Wagner, Yu. Grin, *Int. J. Quantum Chem.* **2006**, *106*, 1499–1507.
[83] M. Kohout, *J. Chem. Soc. Dalton Trans.* **2007**, 135, 43–54.
[84] The Program TB-LMTO-ASA, Version 4.7, O. Jepsen, A. Burkhardt, O. K. Andersen, Max-Planck-Institut für Festkörperforschung, Stuttgart, **2000**.
[85] W. R. L. Lambrecht, O. K. Andersen, *Phys. Rev. B* **1986**, *34*, 2439–2449.
[86] DGRID, Version 4.4, M. Kohout, **2008**.

Received: May 27, 2010
Published online: August 19, 2010

